

# Comparing effective temperatures in standard and Tsallis distributions from transverse momentum spectra in small collision systems

Peng-Cheng Zhang<sup>1,\*</sup>, Pei-Pin Yang<sup>2,†</sup>, Ting-Ting Duan<sup>1,‡</sup>, Hailong Zhu<sup>1,§</sup>, Fu-Hu Liu<sup>1,¶</sup>, Khusniddin K. Olimov<sup>3,4,\*\*</sup>

<sup>1</sup>*Institute of Theoretical Physics & College of Physics and Electronic Engineering,  
State Key Laboratory of Quantum Optics Technologies and Devices &*

*Collaborative Innovation Center of Extreme Optics, Shanxi University, Taiyuan 030006, China*

<sup>2</sup>*Department of Physics, Xinzhou Normal University, Xinzhou 034000, China*

<sup>3</sup>*Laboratory of High Energy Physics, Physical-Technical Institute of Uzbekistan Academy of Sciences,  
Chingiz Aytmatov Str. 2b, Tashkent 100084, Uzbekistan*

<sup>4</sup>*Department of Natural Sciences, National University of Science and Technology  
MISIS (NUST MISIS), Almalyk Branch, Almalyk 110105, Uzbekistan*

**Abstract:** The transverse momentum ( $p_T$ ) spectra of identified light charged hadrons, specifically bosons ( $\pi^\pm$  and  $K^\pm$ ) as well as fermions [ $p(\bar{p})$ ], produced in small collision systems, namely deuteron-gold (d+Au) and proton-proton (p+p) collisions at the top energy of the Relativistic Heavy Ion Collider (RHIC) with a center-of-mass energy of  $\sqrt{s_{NN}} = 200$  GeV, are investigated in this paper. In present study, d+Au collisions are categorized into three centrality classes: central (0–20%), semi-central (20–40%), and peripheral (40–100%) collisions. Various types of distributions, including standard [Bose-Einstein (Fermi-Dirac) and Boltzmann] and Tsallis distributions, are employed to fit the same  $p_T$  spectra to derive different effective temperatures denoted as  $T_{eff}$ . The results indicate that  $T_{eff}$  values obtained from Bose-Einstein, Boltzmann, Fermi-Dirac, and Tsallis distributions exhibit systematically a decreasing trend. Meanwhile, these  $T_{eff}$  values also show a decreasing trend with a decrease in collision centrality. Furthermore, based on the spectra of given particles, a perfect linear relationship is observed between different pairwise combinations of  $T_{eff}$  derived from both Boltzmann and Bose-Einstein (Fermi-Dirac) distributions as well as between Tsallis and Bose-Einstein (Fermi-Dirac) distributions.

**Keywords:** Bose-Einstein (Fermi-Dirac) distribution, Boltzmann distribution, Tsallis distribution, effective temperatures, linear relationship

**PACS numbers:** 25.75.Ag, 25.75.Dw

## I. INTRODUCTION

In high-energy collisions, temperature serves as a crucial concept [1]. It is essential not only for understanding collision mechanisms and particle production [2–6], but also for investigating the critical point associated with phase transitions from hadronic matter to quark-gluon plasma (QGP or quark matter), followed by quick hadronization back to hadronic matter [7–11]. Temperature plays an irreplaceable role in these processes [12–16]. It is widely accepted that if a first-order phase transition occurs with increasing collision energy, the excitation function of temperature will

---

\* 202312602003@email.sxu.edu.cn

† peipinyangshanxi@163.com; peipinyang@xztu.edu.cn

‡ 202312602001@email.sxu.edu.cn

§ Correspondence: zhuhl@sxu.edu.cn

¶ Correspondence: fuhuliu@163.com; fuhuliu@sxu.edu.cn

\*\* Correspondence: khkolimov@gmail.com; kh.olimov@uzsci.net

display either a plateau or saturated structure [17]. Conversely, if the phase transition is characterized by crossover behavior (where changes occur gradually), the excitation function may show a slow upward trend.

There are various types of temperatures associated with high-energy collisions, including, but not limited to, initial temperature, chemical freeze-out temperature, kinetic freeze-out temperature, and effective temperature [18–22]. The initial temperature characterizes the level of excitation within the collision system during its early stage when gluons exist in a saturated state. The chemical (kinetic) freeze-out temperature reflects the degree of excitation during the chemical (kinetic) freeze-out phase when particle ratios (momentum distributions) remain fixed. The effective temperature ( $T_{eff}$  or simply  $T$ ) serves as an overall indicator of thermal motion among particles in all directions, and collective motion within the collision system along the radial direction, at the kinetic freeze-out stage. In this context, thermal motion can be described by the kinetic freeze-out temperature while collective motion is represented by either the average radial flow velocity or its transverse component: the average transverse flow velocity of particles.

It is important to note that these temperatures are model-dependent. A standard baseline is essential for comparing similar types of temperatures derived from different models or distributions. Indeed, distinct types of temperatures necessitate different standard baselines. Investigating these standard baselines for various types of temperatures represents a substantial and challenging endeavor that cannot be adequately addressed within a single paper. Instead, as foundational work in this area, we aim to compare  $T$  values obtained from different models or distributions. Both Bose-Einstein and Fermi-Dirac distributions stem from widely utilized ideal gas model and (Maxwell-)Boltzmann distribution provides their approximate representation. Furthermore considering that Tsallis distribution [23–27] effectively constitutes an infinite multi-component Boltzmann distribution with appropriate weights, these distributions have been selected as illustrative examples to compare their  $T$  for our study.

The extraction of different  $T$  from the same transverse momentum ( $p_T$ ) spectra of identified hadrons in the final state of high-energy collisions originates from different distribution functions. While numerous distributions can be employed to derive a series of  $T$ , these values differ due to their model dependence [28, 29]. In this paper, we utilize standard [Bose-Einstein (Fermi-Dirac) and Boltzmann] and Tsallis distributions to extract distinct  $T$  values from identical experimental  $p_T$  spectra. We also establish the relationships between different pairwise  $T$ .

The structure of this paper is organized as follows: Section 2 describes the formalism associated with various types of distributions. Results and discussions are presented in Section 3. Finally, we provide our summary and conclusions in Section 4.

## II. DIFFERENT TYPES OF DISTRIBUTIONS

For a given emission source of particles produced in high-energy collisions, one may apply different models or distributions to characterize the distribution laws for these particles. The relativistic ideal gas model, widely utilized in thermodynamics, statistical physics, and quantum mechanics, is favored in this study. The invariant yield or particle momentum ( $p$ ) distribution is expressed as [30]

$$\begin{aligned} E \frac{d^3 N}{d^3 p} &= \frac{1}{2\pi p_T} \frac{d^2 N}{dy dp_T} = \frac{1}{2\pi m_T} \frac{d^2 N}{dy dm_T} \\ &= \frac{gV}{(2\pi)^3} E \left[ \exp\left(\frac{E - \mu}{T}\right) \mp 1 \right]^{-1}. \end{aligned} \quad (1)$$

Here,  $N$  represents the particle number,  $g$  denotes the degeneracy factor,  $\mu$  indicates the chemical potential, which is close to zero at high energy,  $E = \sqrt{p^2 + m_0^2} = m_T \cosh y$  refers to energy,  $m_T = \sqrt{p_T^2 + m_0^2}$  is transverse mass,  $m_0$  signifies rest mass,  $y = (1/2) \ln[(E + p_z)/(E - p_z)]$  describes rapidity,  $p_z$  shows the longitudinal momentum of considered particle, and  $V$  represents the volume of a collision system. Additionally,  $-1$  in Eq. (1) corresponds to Bose-Einstein distribution applicable for bosons such as  $\pi^\pm$  and  $K^\pm$  (with  $g = 1$ ), while  $+1$  in Eq. (1) pertains to Fermi-Dirac distribution relevant for fermions like  $p(\bar{p})$  (with  $g = 2$ ).

The density function of momenta  $p$  can be given by expression

$$\frac{dN}{dp} = \frac{2gV}{(2\pi)^2} p^2 \left[ \exp \left( \frac{\sqrt{p^2 + m_0^2} - \mu}{T} \right) \mp 1 \right]^{-1}. \quad (2)$$

The unit-density function of  $y$  and  $p_T$  is written as [30]

$$\begin{aligned} \frac{d^2N}{dydp_T} &= \frac{gV}{(2\pi)^2} p_T \sqrt{p_T^2 + m_0^2} \cosh y \\ &\times \left[ \exp \left( \frac{\sqrt{p_T^2 + m_0^2} \cosh y - \mu}{T} \right) \mp 1 \right]^{-1}. \end{aligned} \quad (3)$$

The density function of  $p_T$  is

$$\begin{aligned} \frac{dN}{dp_T} &= \frac{gV}{(2\pi)^2} p_T \sqrt{p_T^2 + m_0^2} \int_{y_{\min}}^{y_{\max}} \cosh y \\ &\times \left[ \exp \left( \frac{\sqrt{p_T^2 + m_0^2} \cosh y - \mu}{T} \right) \mp 1 \right]^{-1} dy, \end{aligned} \quad (4)$$

where  $y_{\min}$  and  $y_{\max}$  denote the minimum and maximum rapidities, respectively, in the rapidity bin  $[y_{\min}, y_{\max}]$  measured in experiments.

Generally, the experimental range  $[y_{\min}, y_{\max}]$  encompasses mid-rapidity ( $y_C = 0$ ), and the difference  $\Delta y = y_{\max} - y_{\min}$  is not excessively large ( $\Delta y < 1 \sim 2$ ). If the interval  $[y_{\min}, y_{\max}]$  does not include mid-rapidity, it can be shifted to center around mid-rapidity by adding or subtracting a certain quantity. Specifically,  $[y_{\min}, y_{\max}]$  can be directly adjusted to  $[-\Delta y/2, \Delta y/2]$ , allowing for the subtraction of kinetic energy associated with directional motion along the longitudinal axis from the total energy of particles. While radial flow effects do influence  $T$ , contributions from directional motion can be effectively eliminated through shift of rapidity.

In relation to the aforementioned Bose-Einstein (Fermi-Dirac) distribution expressed in terms of invariant yield,  $p$  ( $p_T$ ) density, and unit-density concerning  $y$  and  $p_T$ , removing factors of  $\mp 1$  from these distributions yields approximate expressions suitable for indistinguishable bosons and fermions, namely leading to Boltzmann distribution form. For classical particle emission sources, employing a Boltzmann distribution can be appropriate.

Given the complexity inherent in high-energy collision processes, multiple emission sources can exist for produced particles. Consequently, one might consider a multi-source thermal model [31–35], wherein different sources operate at varying excitation levels or engage distinct reaction mechanisms. The previously discussed Bose-Einstein (Fermi-Dirac) or Boltzmann distributions thus transform into a multi-component distribution that reflects a multi-regional structure within  $p_T$  spectra [36–38].

Due to commonalities and similarities [39–42], as well as universality [43–46] observed in high-energy collisions, various components within this multi-component distribution can adopt analogous forms. Regarding the probability density function of  $p_T$  as an example, the multi-component distribution is expressed as

$$\frac{1}{N} \frac{dN}{dp_T} = \sum_{i=1}^{n_0} k_i \frac{1}{N_i} \frac{dN_i}{dp_T}, \quad (5)$$

where  $i$  denotes the  $i$ -th component in  $n_0$  components,  $N_i$  is the number of particles in the  $i$ -th component, and  $k_i$  is the fraction of the  $i$ -th component. Naturally, the normalization  $\sum_{i=1}^{n_0} k_i = 1$  is obeyed.

The multi-component distribution shows a multi-temperature, i.e., a temperature fluctuation. The average temperature from the multi-component distribution can be calculated as

$$T = \sum_{i=1}^{n_0} k_i T_i, \quad (6)$$

where  $T_i$  is the temperature obtained from the  $i$ -th component. It is worth emphasizing that each component (the  $i$ -th component) in the multi-component  $p_T$  distribution should be the probability density function  $[(1/N_i)dN_i/dp_T]$  which is normalized to 1, but not the general density function  $(dN_i/dp_T)$ , which is normalized to  $N_i$ .

If one considers other types of distributions, but not the probability density function, the multi-component distributions are represented as

$$E \frac{d^3 N}{d^3 p} = \sum_{i=1}^{n_0} E \frac{d^3 N_i}{d^3 p}, \quad (7)$$

$$\frac{dN}{dp} = \sum_{i=1}^{n_0} \frac{dN_i}{dp}, \quad (8)$$

$$\frac{d^2 N}{dy dp_T} = \sum_{i=1}^{n_0} \frac{d^2 N_i}{dy dp_T}, \quad (9)$$

$$\frac{dN}{dp_T} = \sum_{i=1}^{n_0} \frac{dN_i}{dp_T}. \quad (10)$$

The ratio of the contribution of the  $i$ -th component to that of  $n_0$  components is exactly the fraction of the  $i$ -th component,  $k_i$ , which does not appear obviously in these multi-component distributions.

In the case of  $n_0$  being infinitely large, the multi-component Boltzmann distribution results in the Tsallis distribution which has the following forms [23–27]

$$\begin{aligned} E \frac{d^3 N}{d^3 p} &= \frac{1}{2\pi p_T} \frac{d^2 N}{dy dp_T} = \frac{1}{2\pi m_T} \frac{d^2 N}{dy dm_T} \\ &= \frac{gV}{(2\pi)^3} E \left[ 1 + (q-1) \frac{E - \mu}{T} \right]^{-\frac{q}{q-1}}, \end{aligned} \quad (11)$$

$$\frac{dN}{dp} = \frac{2gV}{(2\pi)^2} p^2 \left[ 1 + (q-1) \frac{\sqrt{p^2 + m_0^2} - \mu}{T} \right]^{-\frac{q}{q-1}}, \quad (12)$$

$$\begin{aligned} \frac{d^2 N}{dy dp_T} &= \frac{gV}{(2\pi)^2} p_T \sqrt{p_T^2 + m_0^2} \cosh y \\ &\times \left[ 1 + (q-1) \frac{\sqrt{p_T^2 + m_0^2} \cosh y - \mu}{T} \right]^{-\frac{q}{q-1}}, \end{aligned} \quad (13)$$

$$\begin{aligned} \frac{dN}{dp_T} &= \frac{gV}{(2\pi)^2} p_T \sqrt{p_T^2 + m_0^2} \int_{y_{\min}}^{y_{\max}} \cosh y \\ &\times \left[ 1 + (q-1) \frac{\sqrt{p_T^2 + m_0^2} \cosh y - \mu}{T} \right]^{-\frac{q}{q-1}} dy. \end{aligned} \quad (14)$$

Here,  $q$  is the entropy index, which describes the degree of non-equilibrium of the collision system.

We initially attempted to fit experimental data using a single-component standard distribution, but encountered unsatisfactory results. Subsequently, we employed a two-component standard distribution for fitting; however, the outcomes remained not satisfactory. When utilizing a three-component standard distribution, the results became acceptable. Consequently, it was necessary to adopt the three-component standard distribution. Nevertheless, with the introduction of the entropy index  $q$ , a single Tsallis distribution effectively smoothed temperature fluctuations inherent

in the three-component standard distribution and achieved satisfactory fitting of the experimental data. Therefore, a single-component Tsallis distribution suffices, leaving two- or three-component Tsallis distributions unnecessary.

In the present work, the probability density function  $[(1/N)(dN/dp_T)]$  is used first of all in the calculation of multi-component standard distribution. To fit the experimental invariant yield,  $(1/2\pi p_T)d^2N/dydp_T$ , one needs to use the relation

$$\frac{1}{2\pi p_T} \frac{N_0}{N} \frac{dN}{dp_T} = \frac{1}{2\pi p_T} \int_{y_{\min}}^{y_{\max}} \frac{d^2N}{dydp_T} dy, \quad (15)$$

where  $N_0$  is the normalization constant that is generally the area under the data,  $dN/dp_T$ . In the fit,  $N_0$  is determined by the data itself and has no relation to the model.

For the single-component Tsallis distribution, the unit density function,  $d^2N/dydp_T$ , of  $y$  and  $p_T$  can be utilized. To fit the experimental invariant yield, given by  $(1/2\pi p_T)d^2N/dydp_T$ , one can conveniently multiply  $d^2N/dydp_T$  in Eq. (13) by  $(1/2\pi p_T)$ . This is justified because for small values of rapidity, specifically when  $y \approx 0$ , it follows that  $\cosh y \approx 1$ , due to the narrow rapidity bin defined as  $[y_{\min}, y_{\max}]$ , which encompasses mid-rapidity.

In some cases, to differentiate between various effective temperatures,  $T_{\text{Bose-Einstein}}$  ( $T_{\text{Fermi-Dirac}}$ ),  $T_{\text{Boltzmann}}$ , and  $T_{\text{Tsallis}}$  are used to denote those obtained from their respective distributions: Bose-Einstein (Fermi-Dirac), Boltzmann, and Tsallis distributions. Regardless of the symbol employed in our calculations, while acknowledging that contributions from collective motion within the collision system or flow effects of produced particles may influence the temperature parameter, we aim to derive an effective temperature corresponding to the kinetic freeze-out during evolution of the system.

### III. RESULTS AND DISCUSSION

#### A. Comparison with experimental data

Figures 1–3 present the invariant yields,  $(1/2\pi p_T)d^2N/dydp_T$ , of (a) positive and negative pions ( $\pi^+$  and  $\pi^-$ ), (b) positive and negative kaons ( $K^+$  and  $K^-$ ), as well as (c) protons and antiprotons ( $p$  and  $\bar{p}$ ), produced in mid-rapidity range ( $|y| < 0.5$ ) in deuteron-gold (d+Au) collisions across three centrality percentage classes (central 0–20%, semi-central 20–40%, and peripheral 40–100%) and in proton-proton (p+p) collisions at a center-of-mass energy of  $\sqrt{s_{NN}} = 200$  GeV, which is the top energy per nucleon pair at the Relativistic Heavy Ion Collider (RHIC). The closed and open symbols represent experimental data collected by the STAR Collaboration [47], while the solid and dotted curves correspond to our results for positive and negative hadrons fitted using (i) three-component Bose-Einstein and Boltzmann distributions for  $\pi^+ + \pi^-$  ( $K^+ + K^-$ ), (ii) three-component Fermi-Dirac and Boltzmann distributions for  $p + \bar{p}$ , and (iii) single-component Tsallis distribution for all hadrons mentioned above.

In Figures 1–3, in the fit of three-component Bose-Einstein and Boltzmann distributions for the spectra of  $\pi^+ + \pi^-$  ( $K^+ + K^-$ ), as well as in the fit of three-component Fermi-Dirac and Boltzmann distributions for the spectra of  $p + \bar{p}$ , the normalization constant is  $N_0$  in Eq. (15). At the same time, the single-component Tsallis distribution is applied for the mentioned spectra, where the normalization constant is  $V$  in Eq. (13). Although these two normalization constants could be unified theoretically, they arise from different calculation methodologies. Notably, both  $N_0$  and  $V$  are intrinsically determined by the data itself. It should be noted that  $N_0$  is also applicable to the single-component Tsallis distribution. Similarly,  $V$  can be utilized for both three-component Bose-Einstein (Fermi-Dirac) distributions as well as Boltzmann distributions due to their reliance on identical datasets, albeit minor deviations may occur regarding normalizations.

From Figures 1–3 it becomes evident that both three-component Bose-Einstein (Fermi-Dirac) distributions and Boltzmann distributions provide a good fit to the transverse momentum ( $p_T$ ) spectra, though a considerable number of parameters were applied. Due to the application of these three-component standard distributions, one may obtain

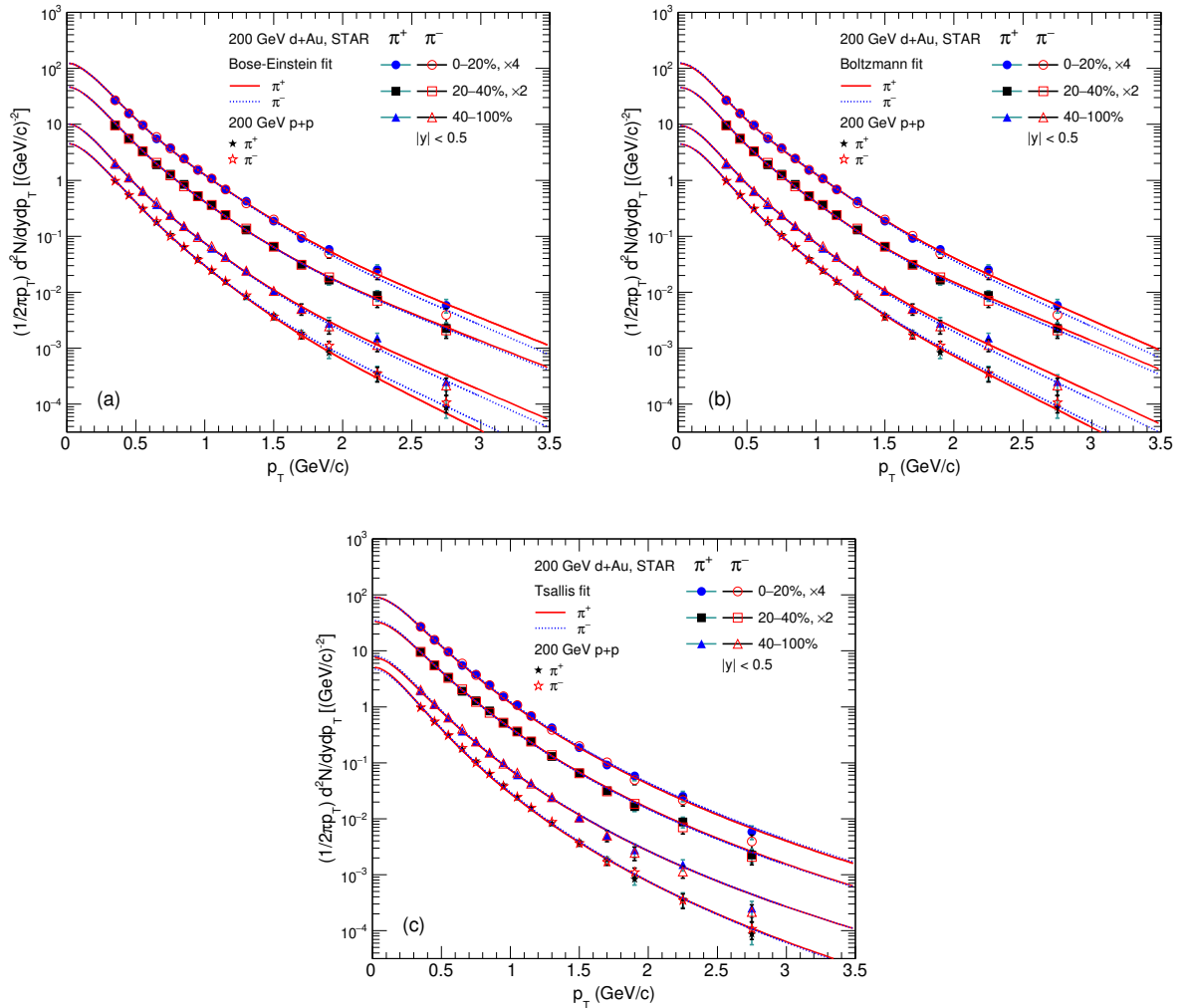


Figure 1. The invariant yields,  $(1/2\pi p_T)d^2N/dydp_T$ , of  $\pi^+$  and  $\pi^-$  produced in  $|y| < 0.5$  in d+Au collisions with three centrality percentages and in p+p collisions at  $\sqrt{s_{NN}} = 200$  GeV. The closed and open symbols represent the experimental data measured by the STAR Collaboration [47]. The solid and dotted curves are our results for  $\pi^+$  and  $\pi^-$  fitted by the (a) three-component Bose-Einstein, (b) three-component Boltzmann, and (c) single-component Tsallis distributions, respectively.

more than one value of temperature. These different values reflect temperature fluctuation from low to high excitation sources in the framework of multi-source thermal model [31–35]. Furthermore, these colorful three- or multi-component standard distributions can effectively be approximated by a single-component Tsallis distribution, where the number of parameters has decreased. The temperature fluctuation existed in the multi-component standard distributions disappears in the single-component Tsallis distribution due to the introduction of index entropy  $q$  in the latter.

## B. Tendencies of free parameters

The relationships between effective temperature  $T_{eff}$  and centrality percentage for the production of (a)  $\pi^\pm$ , (b)  $K^\pm$ , and (c)  $p(\bar{p})$ , obtained from d+Au collisions at  $\sqrt{s_{NN}} = 200$  GeV, are illustrated in Figure 4. The parameter values are derived from Bose-Einstein (Fermi-Dirac, represented by circles), Boltzmann (squares), and Tsallis distributions (triangles). It is important to note that the centrality classes on the horizontal axis are not presented proportionally. Instead, a schematic diagram has been employed to facilitate comparison across different values of centrality percentage. The results depicted in Figure 4 indicate that the values of  $T_{eff}$  derived from the Bose-Einstein,

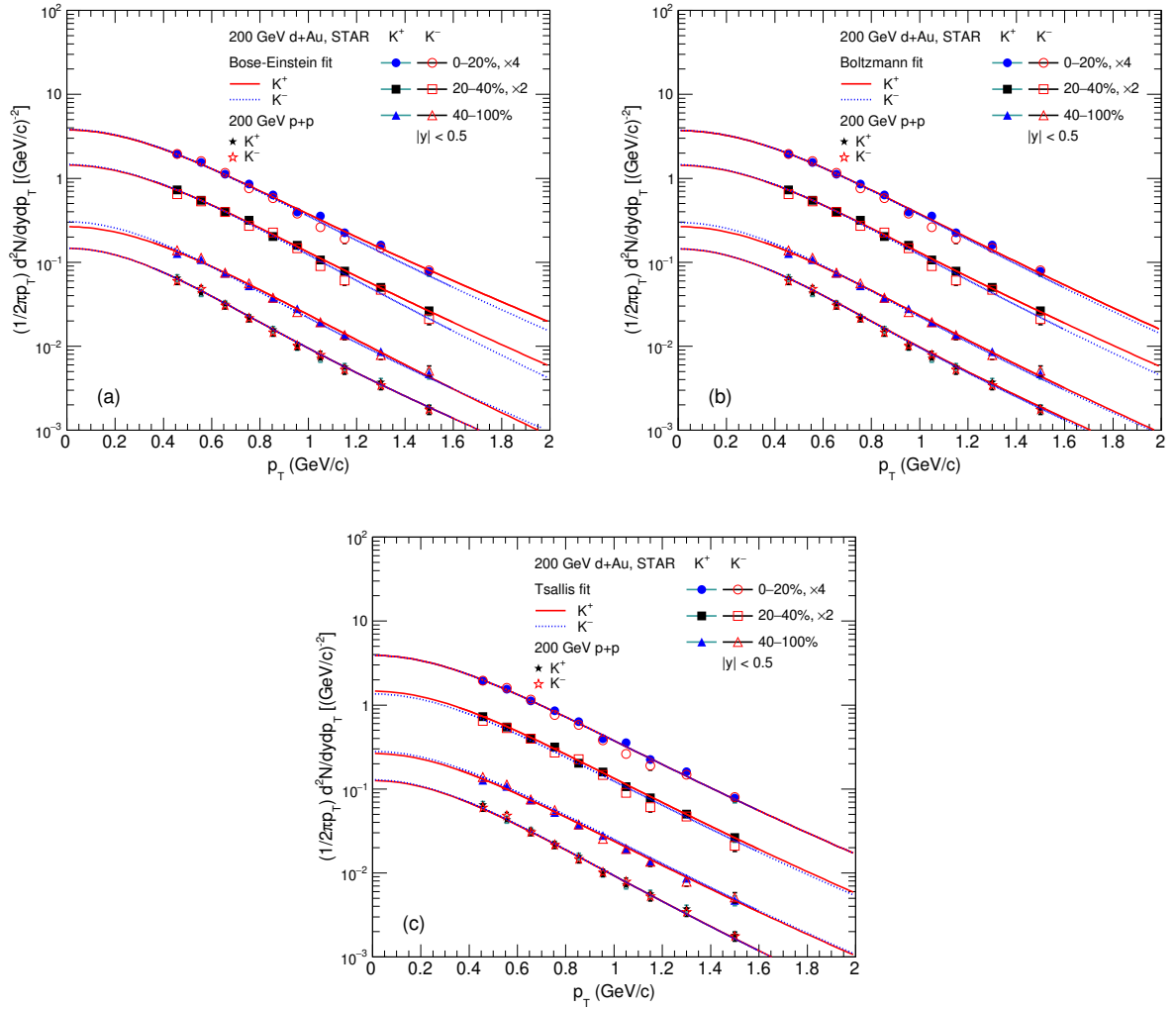


Figure 2. The invariant yields,  $(1/2\pi p_T)d^2N/dydp_T$ , of  $K^+$  and  $K^-$  produced in  $|y| < 0.5$  in d+Au collisions with three centrality percentages and in p+p collisions at  $\sqrt{s_{NN}} = 200$  GeV. The closed and open symbols represent the experimental data measured by the STAR Collaboration [47]. The solid and dotted curves are our results for  $K^+$  and  $K^-$  fitted by the (a) three-component Bose-Einstein, (b) three-component Boltzmann, and (c) single-component Tsallis distributions, respectively.

Boltzmann, Fermi-Dirac, and Tsallis distributions exhibit systematically a decreasing trend. Meanwhile, these  $T_{eff}$  values also show a decreasing trend with a decrease in collision centrality. In practical applications, if we consider  $T_{Bose-Einstein}$  and  $T_{Fermi-Dirac}$  as standard baselines, other temperatures can be evaluated against these benchmarks.

The relative magnitudes of various effective temperatures suggest that  $T_{Boltzmann}$  underestimates  $T_{Bose-Einstein}$  while overestimating  $T_{Fermi-Dirac}$ . This means that  $T_{Bose-Einstein} > T_{Boltzmann}$  for particular bosons and  $T_{Boltzmann} > T_{Fermi-Dirac}$  for particular fermions. The reason is the influence of the value of the last term ( $\mp 1$ ) in the denominator of Eq. (1). Likewise, it appears that the measurement for Tsallis distribution underestimates both baseline temperatures due to the influence of entropy index  $q$ . For particular particles,  $T_{Tsallis}$  is always the minimal one among these effective temperatures. Furthermore, the effective temperatures shown in Figure 4 clearly demonstrate an isospin dependence in absolute values for the production of  $K^\pm$  due to their differing absorption rates within hot and dense systems, as well as for the production of  $p(\bar{p})$  owing to pre-existing protons present in the colliding nuclei. These effective temperatures also indicates the multiple scenarios of kinetic freeze-out with clear mass dependence. Nevertheless, the trends of these effective temperatures are consistent.

Figure 5 presents the relationship between entropy index  $q$  and centrality percentage for the production of  $\pi^\pm$

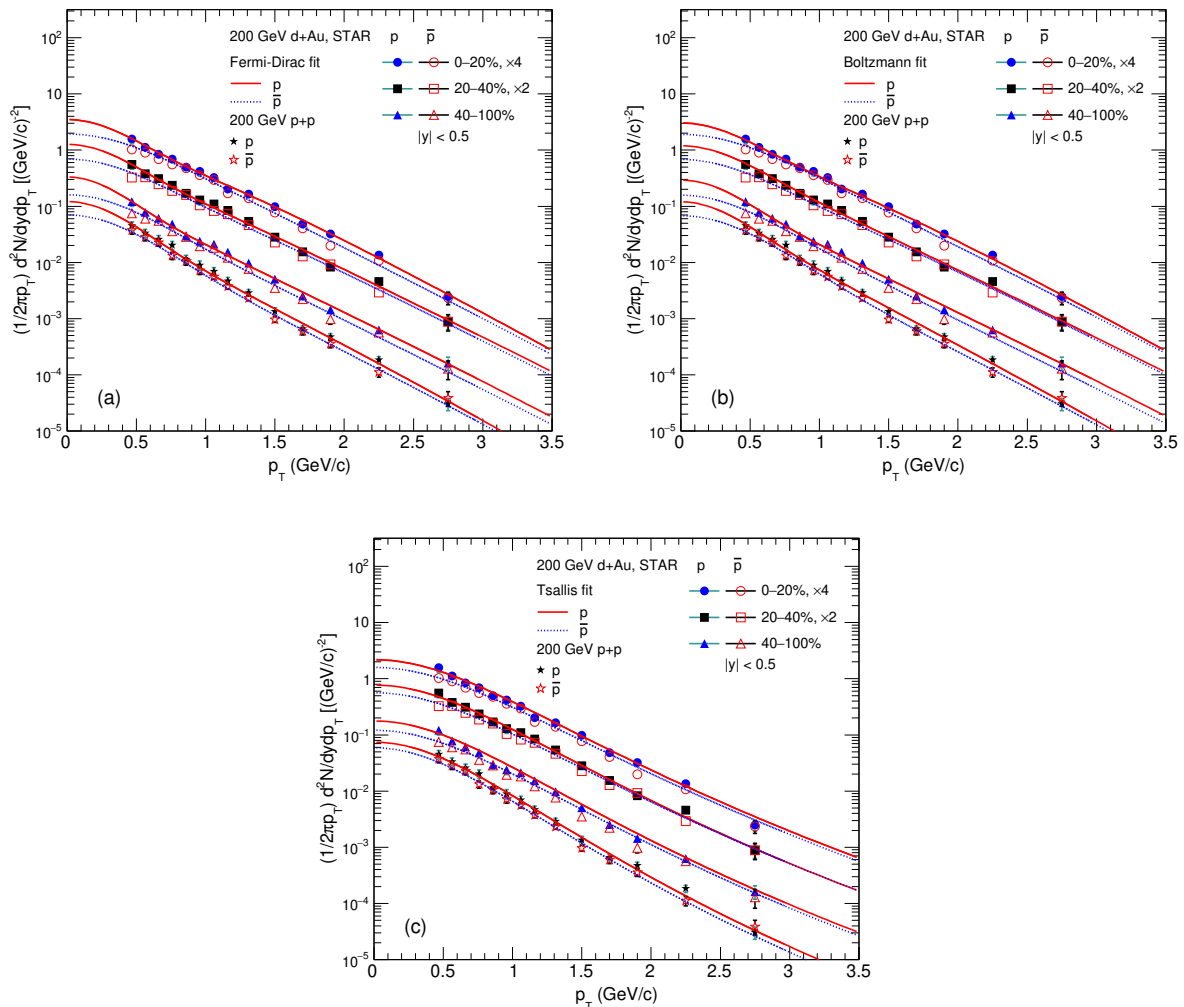


Figure 3. The invariant yields,  $(1/2\pi p_T)d^2N/dydp_T$ , of  $p$  and  $\bar{p}$  produced in  $|y| < 0.5$  in d+Au collisions with three centrality percentages and in p+p collisions at  $\sqrt{s_{NN}} = 200$  GeV. The closed and open symbols represent the experimental data measured by the STAR Collaboration [47]. The solid and dotted curves are our results for  $p$  and  $\bar{p}$  fitted by the (a) three-component Fermi-Dirac, (b) three-component Boltzmann, and (c) single-component Tsallis distributions, respectively.

(circles),  $K^\pm$  (squares), and  $p(\bar{p})$  (triangles). The parameter values are obtained from d+Au collisions at  $\sqrt{s_{NN}} = 200$  GeV, but only using Tsallis distribution. Similar to Figure 4, it should be noted that centrality classes on the horizontal axis are not displayed proportionally; rather, a schematic representation has been provided for comparative purposes. Notably, the values of  $q$  derived from the Tsallis distribution approach unity. This indicates that the collision system is approximately in an equilibrium state. In comparison to peripheral collisions,  $q$  in central collisions is closer to unity, suggesting that central collisions are in a more equilibrated state due to more multi-scatterings in larger participant region. Due to inertia, more massive particles seem more likely to be in equilibrium.

It should be noted that the  $q$  value extracted from  $\pi^\pm$  spectra is larger than those from  $K^\pm$  and  $p(\bar{p})$  spectra for a given centrality. The primary reason lies in the small pion mass. As the lightest hadron (with a mass of approximately 140 MeV), the pion undergoes chemical freeze-out earlier while the system remains in a high-energy density environment far from equilibrium, thereby exhibiting stronger non-extensive features in its momentum distribution ( $q > 1$ ). In contrast, the freeze-out times for protons ( $\sim 938$  MeV) and  $K$  mesons ( $\sim 494$  MeV) occur later, at which point the system transfers into a phase of relative equilibrium evolution ( $q \rightarrow 1$ ). Additionally, due to its small mass and long mean free path, the pion experiences fewer collisions with other system components, making its momentum

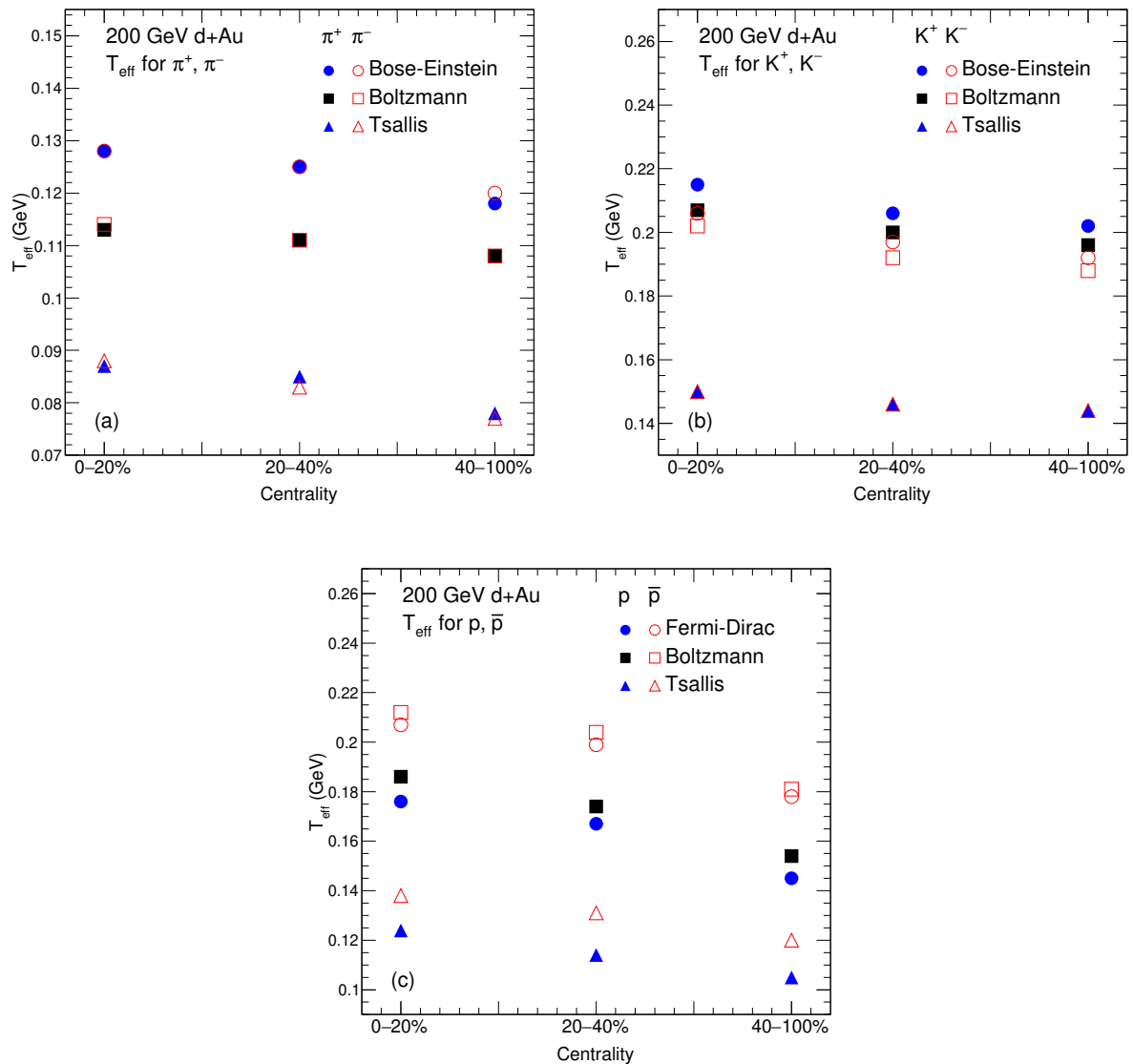


Figure 4. Relationships between effective temperature  $T_{\text{eff}}$  and centrality percentage for productions of (a)  $\pi^\pm$ , (b)  $K^\pm$ , and (c)  $p(\bar{p})$  obtained in d+Au collisions at  $\sqrt{s_{NN}} = 200$  GeV from the Bose-Einstein (Fermi-Dirac) (circles), Boltzmann (squares), and Tsallis distributions (triangles), respectively. Values on the horizontal axis are not given proportionally. The error bars are invisible due to their smaller sizes than the symbol one.

distribution more prone to deviate from equilibrium (manifested as an increase in the  $q$  value). Particles with higher masses tend to thermalize ( $q$  closer to 1) through frequent collisions driven by strong interactions.

Figure 6 illustrates the relationships between (a)/(b)  $T_{\text{Boltzmann}}/T_{\text{Tsallis}}$  and  $T_{\text{Bose-Einstein}}$  for  $\pi^\pm$ , (c)/(d)  $T_{\text{Boltzmann}}/T_{\text{Tsallis}}$  and  $T_{\text{Bose-Einstein}}$  for  $K^\pm$ , as well as (e)/(f)  $T_{\text{Boltzmann}}/T_{\text{Tsallis}}$  and  $T_{\text{Fermi-Dirac}}$  for  $p(\bar{p})$  productions in d+Au collisions at  $\sqrt{s_{NN}} = 200$  GeV. The closed and open symbols represent results for positive and negative hadrons, respectively. From Figure 6, it can be observed that there exists an approximate linear relationship between  $T_{\text{Boltzmann}}$  and  $T_{\text{Bose-Einstein}}$  ( $T_{\text{Fermi-Dirac}}$ ), as well as between  $T_{\text{Tsallis}}$  and  $T_{\text{Bose-Einstein}}$  ( $T_{\text{Fermi-Dirac}}$ ). Naturally, there is also an approximate linear correlation between  $T_{\text{Boltzmann}}$  and  $T_{\text{Tsallis}}$  [48]. To draw accurate conclusions regarding different temperatures with standard baselines, specific fits related to the hadron spectra are necessary.

In contrast to our previous work [48], which examined both  $T_{\text{Boltzmann}}$  and  $T_{\text{Tsallis}}$  based on data from large heavy-ion collision systems, this study focuses on effective temperatures derived from smaller systems such as d+Au and

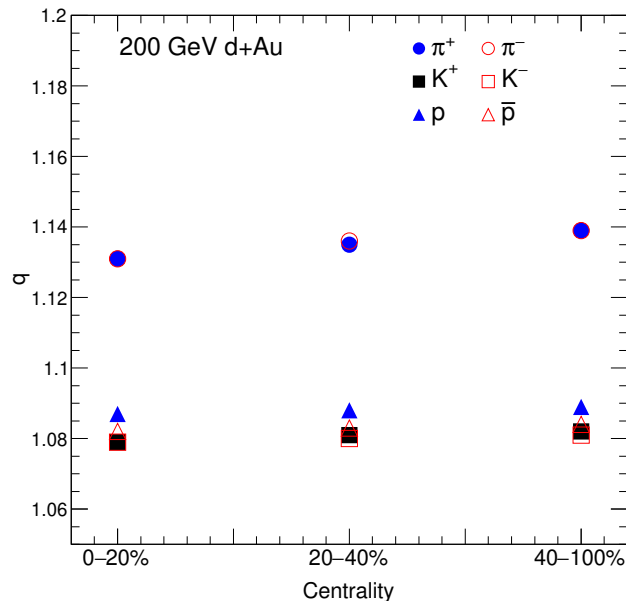


Figure 5. Relationship between entropy index  $q$  and centrality percentage for the production of  $\pi^\pm$  (circles),  $K^\pm$  (squares), and  $p(\bar{p})$  (triangles) obtained in d+Au collisions at  $\sqrt{s_{NN}} = 200$  GeV from the Tsallis distribution. Values on the horizontal axis are not given proportionally. The error bars are invisible due to their smaller sizes than the symbol one.

p+p collisions. By integrating findings from both studies, we may conclude that not only  $T_{\text{Boltzmann}}$  and  $T_{\text{Tsallis}}$ , but also  $T_{\text{Boltzmann}}$  and  $T_{\text{Bose-Einstein}}$  ( $T_{\text{Fermi-Dirac}}$ ), as well as  $T_{\text{Tsallis}}$  and  $T_{\text{Bose-Einstein}}$  ( $T_{\text{Fermi-Dirac}}$ ), have approximate linear relationships based on the data with different centrality classes.

### C. Further discussion

To further investigate the relationship between  $T_{\text{Boltzmann}}$  and  $T_{\text{Bose-Einstein}}$  ( $T_{\text{Fermi-Dirac}}$ ), along with  $T_{\text{Tsallis}}$  and  $T_{\text{Bose-Einstein}}$  ( $T_{\text{Fermi-Dirac}}$ ), we utilize the parameters  $q$  and  $V$  derived from 0–20% d+Au collisions at  $\sqrt{s_{NN}} = 200$  GeV. The results of the Tsallis distributions for production of  $\pi^+$ ,  $K^+$ , and  $p$  are obtained over a range of  $T_{\text{Tsallis}}$  from 0.006 to 0.26 GeV in increasing increments of 0.002, 0.01, or 0.02 GeV, which are subsequently fitted using three-component Bose-Einstein (Fermi-Dirac) and Boltzmann distributions. Selected examples of these Tsallis distributions at specific values of  $T_{\text{Tsallis}} = 0.10, 0.14, 0.18,$  and  $0.22$  GeV, along with their corresponding fitting results, are illustrated in Figures 7(a)–7(d). The meanings of various curves are indicated within each panel. It is evident that the Tsallis distribution can be effectively fitted by three-component Bose-Einstein (Fermi-Dirac) and Boltzmann distributions across a given range of  $p_T$ , although some deviations occur in both low- and high- $p_T$  regions. Similar results for  $\pi^-$ ,  $K^-$ , and  $\bar{p}$  have been observed as shown in Figure 7. However, they are not presented here to avoid redundancy.

The relationships depicted in panels (a)/(b), showing the correlation between  $T_{\text{Boltzmann}}/T_{\text{Tsallis}}$  and  $T_{\text{Bose-Einstein}}$  for  $\pi^+$ ; panels (c)/(d), illustrating the same correlation for  $K^+$ ; as well as panels (e)/(f), representing the correlation between  $T_{\text{Boltzmann}}/T_{\text{Tsallis}}$  and  $T_{\text{Fermi-Dirac}}$  for  $p$  productions, concerning various temperatures based on  $q$  and  $V$  values obtained from 0–20% d+Au collisions at  $\sqrt{s_{NN}} = 200$  GeV—are provided in Figures 8(a)–8(f). In these figures, symbols denote various effective temperatures  $T_{\text{eff}}$  utilized within the three-component Bose-Einstein (Fermi-Dirac) and Boltzmann distributions alongside those used in the Tsallis distribution itself where applicable; the straight lines are the fitting results with the linear equations shown in the panels. Notably, a very good linear relationship for given

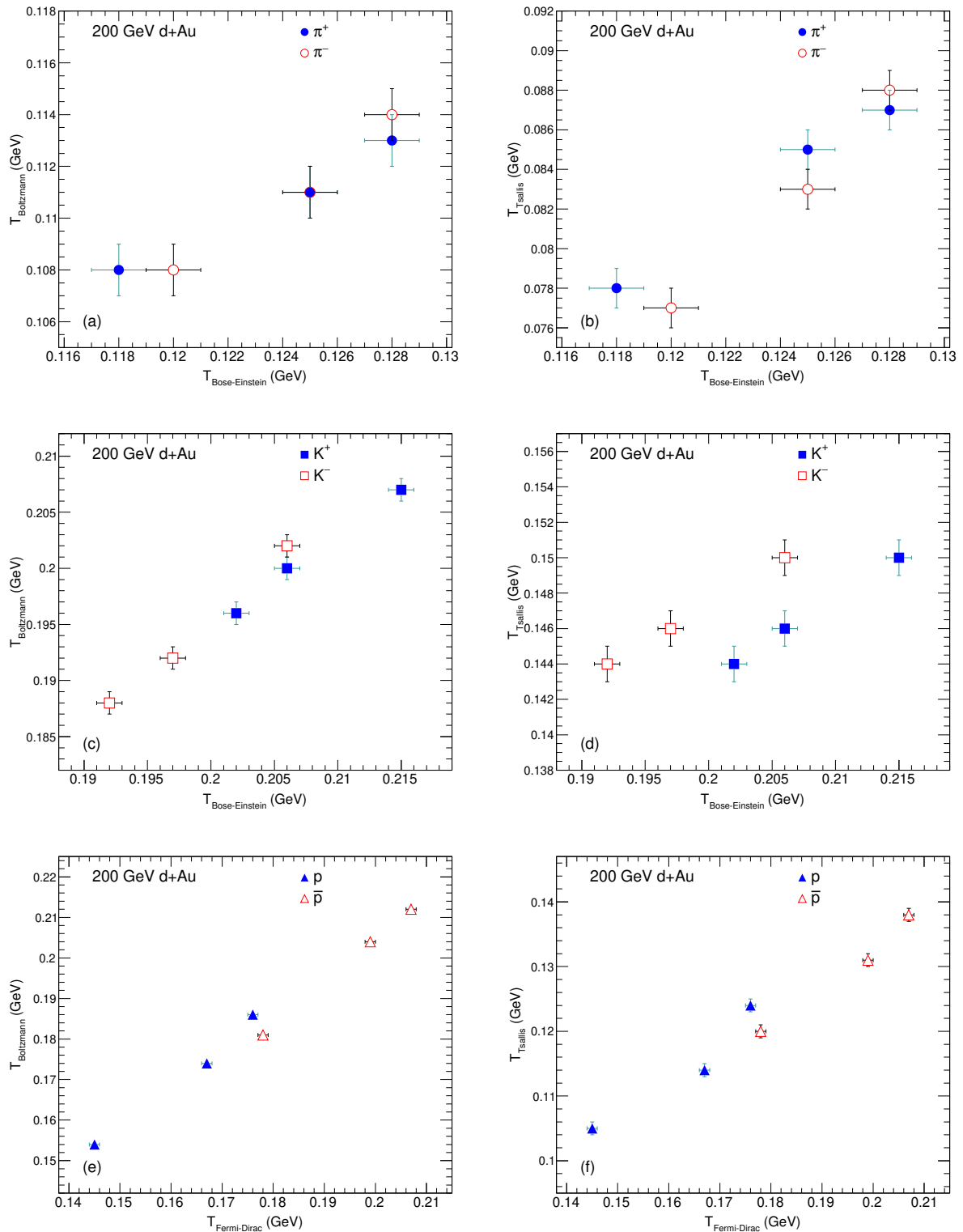


Figure 6. Relationships between (a)/(b)  $T_{\text{Boltzmann}}/T_{\text{Tsallis}}$  and  $T_{\text{Bose-Einstein}}$  for  $\pi^{\pm}$ , (c)/(d)  $T_{\text{Boltzmann}}/T_{\text{Tsallis}}$  and  $T_{\text{Bose-Einstein}}$  for  $K^{\pm}$ , as well as (e)/(f)  $T_{\text{Boltzmann}}/T_{\text{Tsallis}}$  and  $T_{\text{Fermi-Dirac}}$  for  $p$  ( $\bar{p}$ ) productions in d+Au collisions at  $\sqrt{s_{NN}} = 200$  GeV. The closed and open symbols represent the results for positive and negative hadrons, respectively.

correlation and particle spectra can be observed across all six panels presented, though three-component standard distributions are employed to fit the Tsallis distribution.

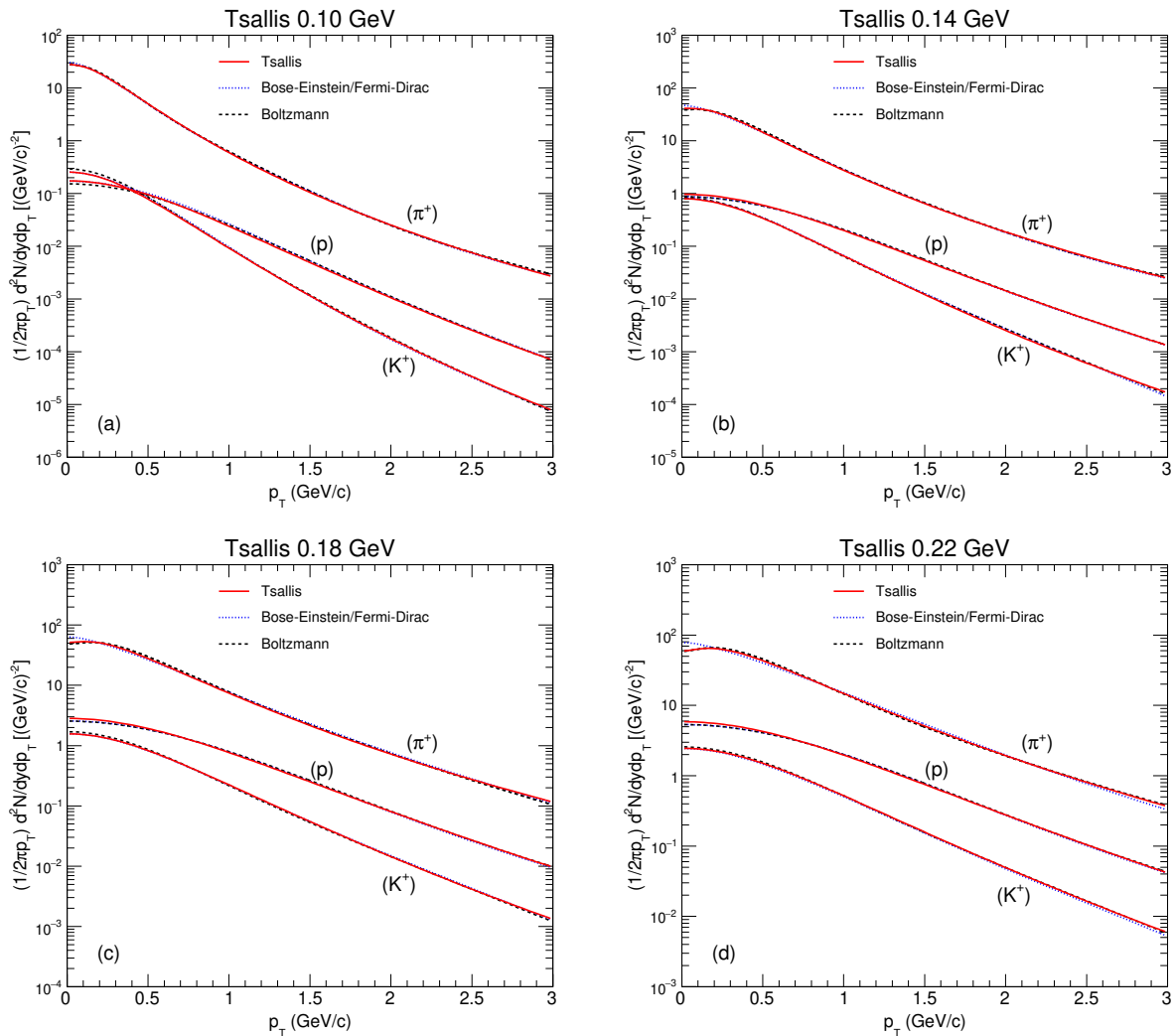


Figure 7. The selected Tsallis distributions with  $T_{\text{Tsallis}} = 0.10$  (a),  $0.14$  (b),  $0.18$  (c), and  $0.22$  GeV (d) and the related fittings by three-component Bose-Einstein (for  $\pi^+$  and  $K^+$ ), Fermi-Dirac (for  $p$ ), and Boltzmann distributions. The values of  $q$  and  $V$  from 0–20% d+Au collisions at  $\sqrt{s_{NN}} = 200$  GeV are used in Tsallis distributions with different  $T_{\text{Tsallis}}$ . The meanings referred to various curves are marked in the panels.

The Bose-Einstein and Fermi-Dirac distributions are widely acknowledged as standard baselines in both classical and modern physics, providing an accurate representation of effective temperature. In contrast, the Boltzmann distribution serves as a reasonable approximation; however, it tends to slightly underestimate (or overestimate) the effective temperature derived from the Bose-Einstein (or Fermi-Dirac) distribution. In addition to these standard distributions, the Tsallis distribution offers an alternative framework. However, it significantly underestimates the effective temperature obtained from three-component Bose-Einstein or Fermi-Dirac distributions due to its incorporation of an entropy index. While other distributions such as the  $q$ -dual distribution [27] and Erlang distribution [31, 32, 35] can be utilized to extract effective temperatures [49, 50], establishing a connection between these extracted effective temperatures and those derived from standard distributions is essential for meaningful comparisons.

Our recent findings [50] indicate an approximate linear relationship or positive correlation—rather than an exact linear correlation—between  $T_{\text{Boltzmann}}$  and  $T_{\text{Bose-Einstein}}$  (or  $T_{\text{Fermi-Dirac}}$ ), as well as between  $T_{\text{Tsallis}}$  and  $T_{\text{Bose-Einstein}}$  (or  $T_{\text{Fermi-Dirac}}$ ) from a comprehensive analysis on the spectra of light hadrons produced in gold-gold (Au+Au) collisions with different centralities over center-of-mass energy range from 7.7 to 200 GeV. The present work shows

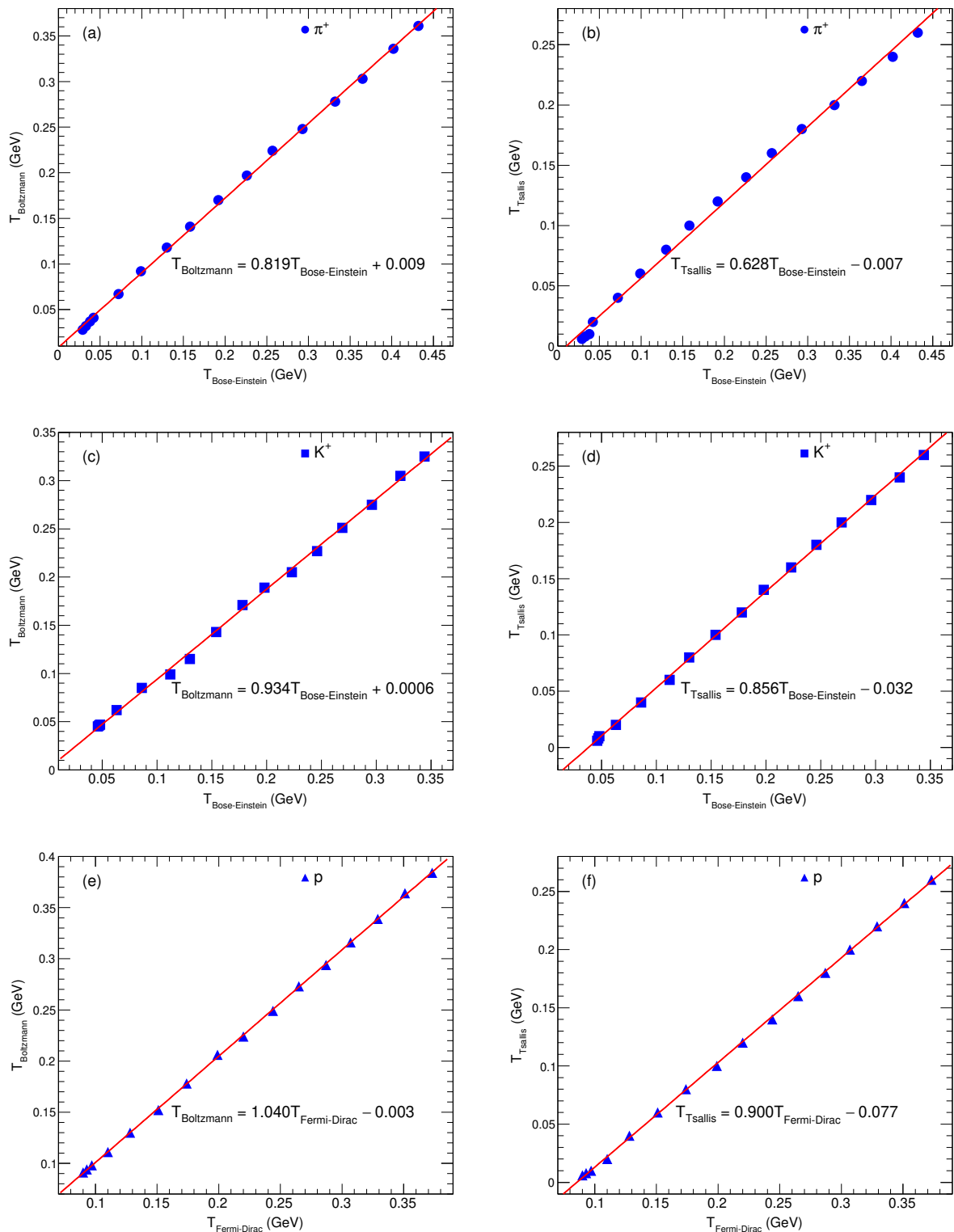


Figure 8. Relationships between (a)/(b)  $T_{\text{Boltzmann}}/T_{\text{Tsallis}}$  and  $T_{\text{Bose-Einstein}}$  for  $\pi^+$ , (c)/(d)  $T_{\text{Boltzmann}}/T_{\text{Tsallis}}$  and  $T_{\text{Bose-Einstein}}$  for  $K^-$ , as well as (e)/(f)  $T_{\text{Boltzmann}}/T_{\text{Tsallis}}$  and  $T_{\text{Fermi-Dirac}}$  for  $p$  productions. The symbols represent the selected 16  $T_{\text{Tsallis}}$  which equals to 0.006, 0.008, 0.01, 0.02, 0.04, 0.06, ..., 0.26 GeV, for which  $q$  and  $V$  are taken from 0–20% d+Au collisions at  $\sqrt{s_{NN}} = 200$  GeV. The straight lines are the fitting results with the linear equations shown in the panels.

better linear correlations based on given particle spectra from 0–20% d+Au collisions at 200 GeV. This outcome is

in line with our earlier expectation [48] of an approximate precise linear relationship among Tsallis and Boltzmann temperatures, from Au+Au collisions at 130 and 200 GeV, as well as lead-lead (Pb+Pb) collisions at 2.76 TeV with various centralities. Regardless of which effective temperature is employed, it is appropriate to adopt the effective temperature derived from standard distributions as a uniform baseline. Numerically, at the same  $\sqrt{s_{NN}}$ , the effective temperature extracted from central nucleus-nucleus collisions exceeds that from peripheral collisions, whereas the effective temperature derived from p+p collisions is closer to and slightly lower than that from peripheral collisions.

Before summarizing and concluding, we want to point out that, when applied to the same dataset, the results obtained using this multi-component ideal gas method are more readily connected to traditional thermodynamics compared to those derived from alternative or more sophisticated models, although a one-to-one correspondence can be established between the two approaches. Moreover, despite high-energy collision processes displaying properties of a small-volume QGP evolution, the behavior of the final-state particles exhibits characteristics of the large-volume gases, validating the rationality of applying the multi-component ideal gas method to study final-state particle behavior. We have analyzed the transverse momentum spectra of various particles across collision processes with different energies and systems, achieving reasonable fitting results [48, 50], which further corroborates the validity of the method employed. During the fitting process, we used a combination of least squares method and leave-one-out cross validation method to determine the optimal parameters.

It is essential to highlight the connection between effective temperature  $T_{eff}$  measurements and the QGP phase transition. While QGP formation occurs on  $\sim 1$  fm/c time scales in high-energy collisions, hydrodynamic evolution preserves memory of initial conditions via flow observables. The  $T_{eff}$  extracted from final-state particle spectra reflects the collective expansion dynamics initiated during the QGP phase. The observed non-monotonic dependence of  $T_{eff}$  on collision energy/centrality provides indirect evidence of the phase transition and potential critical endpoint signatures. Of course, studying phase transitions and critical endpoints cannot be decoupled from temperatures. However, temperatures are model-dependent and necessitate a standardized baseline for meaningful comparisons. Regrettably, no specific criteria or constraints currently exist within the community to ensure consistent comparisons across models. We propose adopting Bose-Einstein and Fermi-Dirac temperatures, extracted from multi-component distributions and widely used in physics for an extended period, as the standard baseline.

We would like to emphasize that this study overcomes the limitations of traditional thermal models—typically confined to large systems—by systematically comparing effective temperatures derived from Bose-Einstein (Fermi-Dirac), Boltzmann, and Tsallis distributions for light hadron transverse momentum spectra in small collision systems at top RHIC energy. This research transcends conventional thermal models, offering an important lens to probe the interrelation between non-equilibrium and local equilibrium phenomena in Quantum Chromodynamics (QCD) systems. Indeed, the analysis reveals the coexistence of pronounced non-equilibrium effects for single-event in small systems and local thermal equilibrium for lots of events. While quantum statistics (Bose-Einstein/Fermi-Dirac) and Tsallis non-extensive statistics diverge in describing spatiotemporally constrained systems, their applications highlight the persistence of partial thermalization. This dual behavior challenges the universality of equilibrium assumptions and underscores the need for hybrid statistical frameworks to decode the QCD medium's evolution.

The interplay between Tsallis entropy index  $q$  and effective temperatures  $T$  establishes a quantitative link between microscopic quantum fluctuations (e.g., fractal phase-space structures) and macroscopic thermodynamic observables. Such correlations suggest fractal thermalization as a potential feature of QCD matter under extreme conditions. Furthermore, anchoring effective temperatures to Bose-Einstein (Fermi-Dirac) baselines provides a foundational reference for cross-model comparisons, enabling unified interpretations of temperature fluctuations across statistical paradigms. By demarcating the dominance of quantum statistics at low  $p_T$  and Tsallis non-extensivity at high  $p_T$ , this work guides the design of precision momentum spectrum measurements at RHIC, Large Hadron Collider (LHC), and future Electron-Ion Collider (EIC) facilities. These insights can not only provide reference for optimizing detector design, but also improve hydrodynamic and transport models to more accurately capture non-equilibrium phase transitions. Ultimately, the integration of multi-model perspectives can reshape theoretical benchmarks for thermalization

criteria, and advance the exploration of exotic quantum matter in high-energy collisions and early-universe.

#### IV. SUMMARY AND CONCLUSIONS

The transverse momentum spectra of  $\pi^\pm$ ,  $K^\pm$ , and  $p(\bar{p})$  produced in d+Au and p+p collisions at  $\sqrt{s_{NN}} = 200$  GeV, measured by the STAR Collaboration, are analyzed using three-component Bose-Einstein (Fermi-Dirac), three-component Boltzmann, and single-component Tsallis distributions. The effective temperatures  $T_{eff}$  and entropy index  $q$  derived from the spectra of different particles reveal a multi-scenario approach to kinetic freeze-out. Due to the significantly high yields of  $\pi^\pm$ , the average parameters weighted across different particles closely resemble those obtained from the spectra of  $\pi^\pm$ .

Our findings indicate that the values of  $T_{eff}$  derived from three-component Bose-Einstein, Boltzmann, and Fermi-Dirac distributions, as well as from single-component Tsallis distribution, exhibit systematically a decreasing trend. Meanwhile, these  $T_{eff}$  values also show a decreasing trend with a decrease in collision centrality. In practical applications, if we consider  $T_{Bose-Einstein}$  and  $T_{Fermi-Dirac}$  as standard baselines for comparison with other temperature measurements, it is observed that  $T_{Boltzmann}$  underestimates  $T_{Bose-Einstein}$  while overestimating  $T_{Fermi-Dirac}$ , whereas  $T_{Tsallis}$  underestimates both temperatures. Furthermore, a nearly perfect linear relationship exists between  $T_{Boltzmann}$  and  $T_{Bose-Einstein}$  ( $T_{Fermi-Dirac}$ ), as well as between  $T_{Tsallis}$  and  $T_{Bose-Einstein}$  ( $T_{Fermi-Dirac}$ ), based on given particle spectra.

As one moves from central to peripheral d+Au collisions, there is a slight decrease in the values of  $T_{eff}$  obtained from various distributions for emissions across different particles. Concurrently, values of  $q$  extracted from the Tsallis distribution show a gradual increase for emissions involving different particles. Notably, parameters obtained from p+p collisions exhibit similarities to those observed in peripheral d+Au collisions. This similarity arises from nearly identical energy depositions, comparable initial-state geometries, and minimized hadronic re-scattering effects in both p+p and d+Au collisions systems.

#### Acknowledgments

The work of Shanxi group was supported by National Natural Science Foundation of China under Grant No. 12147215, Fundamental Research Program of Shanxi Province under Grant No. 202303021221071, Shanxi Scholarship Council of China and the Fund for Shanxi “1331 Project” Key Subjects Construction. The work of P.-P.Y. was supported by Fundamental Research Program of Shanxi Province under Grant No. 202203021222308, Doctoral Scientific Research Foundations of Shanxi Province and Xinzhou Normal University, and Academic Leading Specialist Project of Xinzhou Normal University under Grant Nos. 2024RC10 and 2024RC10B. The work of K.K.O. was supported by the Agency of Innovative Development under the Ministry of Higher Education, Science and Innovations of the Republic of Uzbekistan within the fundamental project No. F3-20200929146 on analysis of open data on heavy-ion collisions at RHIC and LHC.

#### Data availability

The data used to support the findings of this study are included within the article and are cited at relevant places within the text as references.

#### Declarations

#### Ethical approval

The authors declare that they are in compliance with ethical standards regarding the content of this paper.

#### Conflict of interest

The authors declare that there are no conflict of interest regarding the publication of this paper. The funding agencies have no role in the design of the study; in the collection, analysis, or interpretation of the data; in the writing of the manuscript; or in the decision to publish the results.

- 
- [1] T S Biró *Is there a temperature? conceptual challenges at high energy, acceleration and complexity* (New York, USA: Springer New York) (2011)
- [2] M Waqas and G X Peng *Entropy* **23** 488 (2021)
- [3] K Attri, M K Singh and P K Khandai *Indian J. Phys.* **99** 1091–1096 (2025)
- [4] S Sadhu and P Ghosh *Phys. Rev. D* **99** 034020 (2019)
- [5] M K Singh *Indian J. Phys.* **99** 3429–3434 (2025)
- [6] R Sahoo, A N Mishra, N K Behera and B K Nandi *Adv. High Energy Phys.* **2015** 612390 (2015)
- [7] P Tribedy for the STAR Collaboration *Nucl. Phys. A* **904–905** 463c–466c (2013)
- [8] J I Kapusta, R. Venugopalan and A P Vischer *Phys. Rev. C* **51** 901–910 (1995)
- [9] P Braun-Munzinger and J Stachel *Nucl. Phys. A* **606** 320–328 (1996)
- [10] J Alam, S Sarkar, P Roy, T Hatsuda and B Sinha *Ann. Phys.* **286** 159–248 (2001)
- [11] S A Bass and A Dumitru *Phys. Rev. C* **61** 064909 (2000)
- [12] K Okamoto and C Nonaka *Phys. Rev. C* **98** 054906 (2018)
- [13] J Alam *Pramana – J. Phys.* **60** 663–674 (2003)
- [14] M Ishihara *Phys. Rev. C* **64** 064903 (2001)
- [15] M Waqas, G X Peng, M Ajaz, A H Ismail, Z Wazir and L L Li *J. Phys. G* **49** 095102 (2022)
- [16] D Atta, V Singh and D N Basu, *Indian J. Phys.* **98** 4243–4249 (2024)
- [17] M Badshah, H I Alrebdi, M Waqas, M Ajaz and M B Ammar *Eur. Phys. J. A* **60** 139 (2024)
- [18] M Csanad and I Majer *Cent. Eur. J. Phys.* **10** 850–857 (2012)
- [19] P Braun-Munzinger, J Stachel and C Wetterich *Phys. Lett. B* **596** 61–69 (2004)
- [20] F A Flor, G Olinger and R Bellwied *Phys. Lett. B* **834** 137473 (2022)
- [21] M Waqas, G X Peng, Z Wazir and H L Lao *Int. J. Mod. Phys. E* **30** 2150061 (2021)
- [22] Y B Ivanova and V N Russkikh *Eur. Phys. J. A* **37** 139–142 (2008)
- [23] C Tsallis *J. Stat. Phys.* **52** 479–487 (1988)
- [24] C Tsallis *Braz. J. Phys.* **39** 337–356 (2009)
- [25] T S Biró, G Purcsel and K Ürmössy *Eur. Phys. J. A* **40** 325–340 (2009)
- [26] J Cleymans and M W Paradza *Physics* **2** 654–664 (2020)
- [27] A S Parvan *Eur. Phys. J. A* **56** 106 (2020)
- [28] H Zheng and L L Zhu *Adv. High Energy Phys.* **2016** 9632126 (2016)
- [29] Z B Tang, Y C Xu, L J Ruan, G van Buren, F Q Wang and Z B Xu *Phys. Rev. C* **79** 051901(R) (2009)
- [30] J Cleymans and D Worku *Eur. Phys. J. A* **48** 160 (2012)
- [31] F-H Liu *Nucl. Phys. A* **810** 159–172 (2008)
- [32] F-H Liu and J-S Li *Phys. Rev. C* **78** 044602 (2008)
- [33] F-H Liu *Phys. Rev. C* **78** 014902 (2008)
- [34] F-H Liu, B K Singh and N N Abd Allah *Proceedings of the 14th International Symposium on Very High Energy Cosmic Ray Interactions* (Weihai, China, 2006) (Nucl. Phys. B (Proc. Suppl.) 175–176) (eds) K S Cheng, R Engel, Y Q Ma, B Pattison, Z G Yao and Q Q Zhu (The Netherlands: Elsevier Press) pp 54–57 (2008)
- [35] J-Y Chen, M-Y Duan, F-H Liu and K K Olimov *Indian J. Phys.* **98** 2493–2505 (2024)

- [36] M Suleymanov *Int. J. Mod. Phys. E* **27** 1850008 (2018)
- [37] M Suleymanov *Int. J. Mod. Phys. E* **28** 1950084 (2019)
- [38] M Suleymanov *Phys. Part. Nucl.* **54** 693–702 (2023)
- [39] A N Mishra, A Ortiz and G Paic *Phys. Rev. C* **99** 034911 (2019)
- [40] E K G Sarkisyan and A S Sakharov *The 35th International Symposium on Multiparticle Dynamics (ISMD 05) and 1st Workshop on Particle Correlations and Femtoscopy (WPCF 2005)* (Kromeriz, Czech Republic, 2005) (AIP Conf. Proc. 828) (eds) V Simak, M Sumbera, S Todorova-Nova and B Tomasik (New York: AIP) pp 35–41 (2006)
- [41] A N Mishra, R Sahoo, E K G Sarkisyan and A S Sakharov *Eur. Phys. J. C* **74** 3147 (2014). (**Erratum Eur. Phys. J. C 75 70 (2015)**)
- [42] E K G Sarkisyan and A S Sakharov *Eur. Phys. J. C* **70** 533–541 (2010)
- [43] E K G Sarkisyan, A N Mishra, R Sahoo and A S Sakharov *Phys. Rev. D* **93** 054046 (2016). (**Erratum Phys. Rev. D 93 079904 (2016)**)
- [44] E K G Sarkisyan, A N Mishra, R Sahoo and A S Sakharov *Phys. Rev. D* **94** 011501(R) (2016)
- [45] E K G Sarkisyan, A N Mishra, R Sahoo and A S Sakharov *EPL* **127** 62001 (2019)
- [46] P Castorina, A Iorio, D Lanteri, H Satz and M Spousta *Phys. Rev. C* **101** 054902 (2020)
- [47] J Adams, C Adler, M M Aggarwal et al [STAR Collaboration] *Phys. Lett. B* **616** 8–16 (2005)
- [48] Y-Q Gao and F-H Liu *Indian J. Phys.* **90** 319–334 (2016)
- [49] F-H Liu, Y-Q Gao, T Tian and B-C Li *Eur. Phys. J. A* **50** 94 (2014)
- [50] T-T Duan, P-P Yang, P-C Zhang, H-L Lao, F-H Liu and K K Olimov *Eur. Phys. J. Plus* **139** 1069 (2024)